

Creating a Predictive Model Using Electroencephalography to Discriminate Between Right and Left Stepping

C. Gaina Ghiroaga^{1,3}, A. Kline^{1,2,3}, D. Pittman², B. Goodyear^{1,2}, T. Kline¹, J. Ronsky^{1,3}

¹Biomedical Engineering Program, University of Calgary, ²Hotchkiss Brain Institute,

³McCaig Institute, calin.gainaghiroaga@ucalgary.ca

INTRODUCTION

Neuromotor control of walking has been studied using several different modalities, including electroencephalography (EEG). Previous work has isolated gait-related movement artifacts in the EEG data [1]; while Presacco et al. demonstrated capability in decoding intra-limb and inter-limb kinematics from EEG data [2], others distinguished areas of activation in the brain between executed and imagined walking [3]. Studies to isolate between left and right steps during executed [2] and imagined walking has only started to be performed. To validate this, we looked at specific frequency bands that are of importance for neuromotor control: the alpha (8 – 12 Hz) and beta (12 – 30 Hz) frequency bands. These were found to be most commonly associated with lower limb locomotion in EEG [3]. The electrodes that we were interested in are the C1 and C2 electrodes, located on top of the head where the motor cortex is located. The objectives of this study were to determine if left and right steps are differentiable for executed walking. The hypothesis of this study is that it is possible to differentiate between left and right steps in EEG data. This was done by determining if there was any significance between right vs. left leg lift using the alpha and beta frequency bands for the C1 and C2 electrodes based on a 10-20 EEG electrode system.

METHODS

The inclusion criteria for the participants included being an adult male, ages 20-30 years old, without any neurological deficits or past knee injuries. EEG data was collected for n=9 participants using a 64 electrode EEG cap for one timepoint at a sampling frequency of 1000 Hz. The participants were presented a stimulus video where they simulated executed walking in a supine position. Left and right steps were repeated 60 times each. The data were processed using Compumedics Neuroscan® and a custom Matlab® code. This was done to transform the data into the frequency domain using a Fourier transform, where the powers for the alpha and beta frequency band were obtained. Multi-level modeling (MLM) analyses using the GEE program of IBM SPSS® was run for each electrode and frequency, and for both executed and imagined states. MLM was used when the predictor variables are at different hierarchical levels, as was the case in this study. The Wald test signifies whether there is any significant relationship between leg movement and the powers of the alpha and beta frequency bands for the C1 and C2 electrodes.

RESULTS

Results from the Wald test where $p < 0.05$, are considered significant. The significance levels for the C1 electrode in the beta frequency band for executed walking were $p = 0.09$. The significance levels for the C2 electrode in the alpha band for executed walking were $p = 0.01$. This can be seen in Fig. 1.

REFERENCES

- [1] J. E. Kline, H. J. Huang, K. L. Snyder, and D. P. Ferris, *J. Neural Eng.*, vol. **12**, no. 4, p. 46022, 2015.
- [2] A. Presacco, L. W. Forrester, and J. L. Contreras-Vidal, "*IEEE Trans. Neural Syst. Rehabil. Eng.*", vol. 20, no. 2, pp. 212–219, 2012.
- [3] J. Yinlai, S. Wang, and R. Tan, *J. Infrared Spectroscopy*, 2012

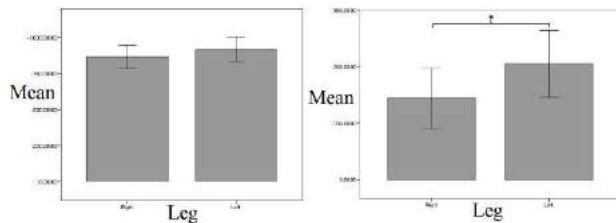


Figure 1. The mean power in beta (left) and alpha (right) frequency bands are shown for electrodes C1 and C2 for left and right leg movements

DISCUSSION AND CONCLUSIONS

Our results show that leg movement is significantly related to certain frequency bands at the C2 electrode for executed walking. The alpha band at the C2 electrode was found to be significant during executed cases; therefore, this may be the most useful measure of differentiating left from right steps. Our results indicate it is possible to differentiate between left and right steps for an executed task. Therefore, the objective was completed, and the hypothesis supported. The medical impact of differentiating between left and right steps is that the classification of left and right steps combined with an exoskeleton or prosthesis will allow motor compromised individuals to walk again using these devices.



MECHANICAL FATIGUE OF BOVINE CORTICAL BONE IN TENSION AND COMPRESSION

Annette Harvey, Lindsay Loundagin, W. Brent Edwards

¹Human Performance Lab, Faculty of Kinesiology, ^{1,2}McCaig Institute for Bone and Joint Health,

^{1,2,3}Cumming School of Medicine, University of Calgary, aharvey1@uvic.ca

INTRODUCTION

Cyclic loading of bone causes microdamage to accumulate, which may eventually lead to fatigue fracture. The damage developed during cyclic loading is dependent on loading mode. When loaded in tension, microcracks initiate easily but toughening mechanisms hinder further crack growth, whereas in compression, microcracks are difficult to initiate but propagate rapidly [1]. Loading mode differences between damage morphology and progression may also depend on underlying bone microarchitecture [2]. While the role that loading mode and microarchitecture play in the development of fatigue damage has been investigated, how these factors ultimately influence fatigue life is unknown. The purpose of this study was to quantify the effect of microarchitecture on the fatigue life of bovine cortical bone cyclically loaded in compression and tension.

METHODS

Seventeen cylindrical bone samples from bovine femora and tibiae were machined into a waisted geometry with a central gauge section 7 mm in length and 5.25 mm in diameter. All samples were imaged using Scanco microCT 100 (Scanco Medical AG, Switzerland) with a resolution of 5 μ m. The microarchitecture was quantified by median canal diameter (Ca.Dm), median canal separation (Ca.Sp), and porosity.

Mechanical fatigue testing was performed on an Instron Electropuls E3000 test frame (Instron, Norwood, MA). Samples were cyclically loaded in

either zero-compression (n=9) or zero-tension (n=8) at a frequency of 4.35 Hz. The loading magnitude was chosen as 45% of the ultimate strength as previously reported [3] for each loading mode, resulting in compressive and tensile stresses of 95 and 73 MPa, respectively. Fatigue life was quantified as the number of loading cycles until failure, which corresponded with complete fracture in all cases. Pearson product-moment correlation was used to determine the relationships between microarchitectural features and fatigue life ($\alpha=0.05$).

RESULTS

When loaded in compression, Ca.Dm ($r=-0.738$, $p=0.023$) and porosity ($r=-0.639$, $p=0.064$) had a strong negative correlation with fatigue life (Fig. 1a), but no relationship was observed for Ca.Sp ($r=0.078$, $p=0.842$). In tension, porosity ($r=0.811$, $p=0.014$) demonstrated a strong positive correlation with fatigue life (Fig. 1b); however, Ca.Dm ($r=0.263$, $p=0.529$) and Ca.Sp ($r=-0.128$, $p=0.763$) were not significant predictors of fatigue life.

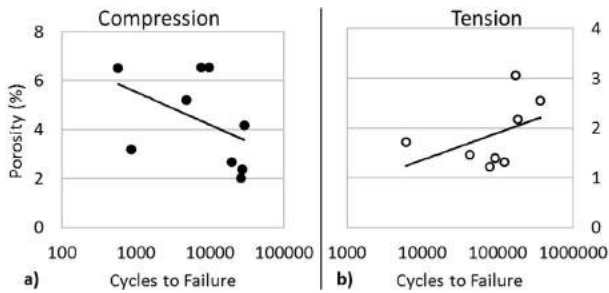


Figure 1: The effect of bone porosity on fatigue life was (a) negatively correlated in compression, but positively correlated in tension (b).

DISCUSSION AND CONCLUSIONS

These results suggest that microarchitecture influences the fatigue behavior of bone that is dependent on loading mode. Bone porosity explains a large amount of the variance in fatigue life for both compression and tension (Fig. 1), however, the opposing correlations may be indicative of different damage mechanisms occurring during each mode of loading. For instance, a higher porosity may be associated with a greater number of canals, and therefore more osteonal cement lines, which provide opportunity for cracks growing in tension to be deflected and increase the fatigue life. Conversely, cracks propagating under cyclic compression are not as easily deflected, such that a higher porosity effectively reduces the net cross-sectional area and increases the local stress level, resulting in a lower fatigue life. Future work will image damage associated with cyclic loading to further elucidate the mechanisms of fatigue failure of bone.

REFERENCES

1. George & Vashishth. *J Orthop Res.* **23**: 1047-53, 2005.
2. Carter & Hayes. *Clin Orthop Relat Res.* **127**:265-74, 1977.
3. Vashishth et al. *J Orthop Res.* **19**: 414-420, 2001



INSTABILITY OF MUSCLE SARCOMERES DURING PROGRESSIVE DEACTIVATION

Shaelyn Jones², Tim Leonard¹, Azim Jinha¹, and Walter Herzog¹

¹Human Performance Lab, University of Calgary, ²Biomedical Engineering Program, University of Calgary
shaelyn.jones@ucalgary.ca

INTRODUCTION

The smallest functional unit of muscle is the sarcomere. The active forces and passive forces generated by the muscle are both dependent on the length of the sarcomere [1]. Active force is generated through cross-bridge cycling (the interaction between actin and myosin), while passive force is controlled by the protein titin. It has been proposed that an instability of sarcomeres can contribute to injuries in muscle due to sarcomeres being arranged in-series. This arrangement makes up a myofibril, where the same force must be sustained along the myofibril and sarcomeres that are weaker than their neighbours are likely to overlengthen due to their inability to produce larger active forces. This instability causes rapid lengthening of the sarcomere (termed “popping”) until passive forces must maintain the force, thus resulting in damage to the sarcomere [2]. The objective of this study was to analyze the change in length of each sarcomere in a single myofibril during successive activation and deactivation, and observe whether the weaker sarcomeres overlengthen, as previously stated, or can sustain the in-series force. We hypothesize that weaker sarcomeres will not overlengthen because this will be prevented by titin.

METHODS

Single myofibrils were attached on one end to a glass needle while the other end of the myofibril was attached to a cantilever pair used to measure force. During the experiment, high resolution video

data was continuously recorded and was then analyzed using a custom MATLAB code. Initially, the myofibril was in a relaxed state. Myofibril length was adjusted until an average sarcomere length (SL) of 2.4 μm was obtained. An activating solution was then added and once the myofibril reached full activation, a stream of relaxing solution flowed in from the left side of the myofibril. The composition of the solutions has been previously reported [3]. This caused a progressive deactivation (weakness) along the myofibril starting from the left and moving towards the right until full deactivation.

RESULTS

Figure 1 depicts a typical experiment where the mean SL before activation (panel 1) was 2.3 μm . Upon full activation (panel 2), the mean SL was 2.1 μm and the measured stress was 171nN/ μm^2 . The addition of the relaxing solution at 17s (panel 3) resulted in the rapid lengthening of the first and second sarcomere. Sarcomere 1 lengthened from a SL of 2.03 μm to 2.56 μm , while sarcomere 2 lengthened from a SL of 2.29 μm to 2.47 μm . At 18s (panel 4), 5 more sarcomeres “popped”. The recorded stress was 83nN/ μm^2 and the mean SL of the relaxed sarcomeres was 2.65 μm while the “unpopped” sarcomeres had a mean SL of 2.15 μm .

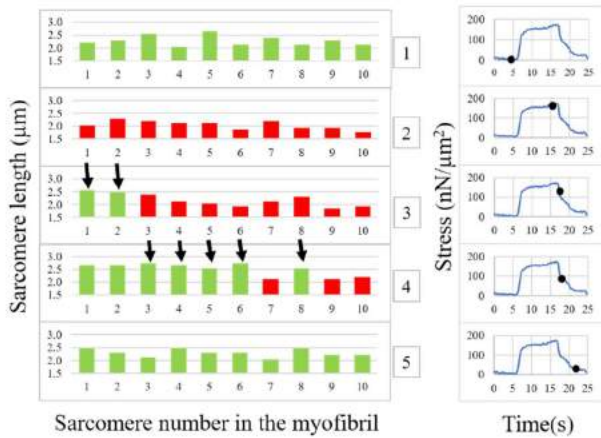


Figure 1: The effect of bone porosity on fatigue life was (a) negatively correlated in compression, but positively correlated in tension (b).

DISCUSSION AND CONCLUSIONS

19 sarcomeres were observed where the deactivation resulted in a rapid lengthening of the sarcomere, but “popping” was not observed for all test conditions. Considering instability theory, one would expect these sarcomeres to overlengthen to nearly double their initial length. It is presumed that titin is sustaining the tension in the passive sarcomeres. In conclusion, the hypothesis was correct and weaker sarcomeres do not overlengthen presumably due to the “stiffening” of titin.

REFERENCES

1. Gordon AM et al., *J. Physiol.* **184**:170-92, 1966.
2. Morgan DL, *Biophys J.* **57**:209-221, 1990.
3. Joumaa V et al., *Eur J. Physiol.* **455**:367-371, 2007.



INVESTIGATING RABBIT ACHILLES AND SUPRASPINATUS TENDON ENTHESES UNDER TENSILE LOAD

Saad Khurshid^{1,2*}, Jansher Chatha^{1,2*}, Johnathan Sevick², May Chung², David Hart², Nigel Shrive^{1,2}

¹Department of Civil Engineering, University of Calgary, ²McCaig Institute of Bone and Joint Health, University of Calgary, *Both contributed equally to the work, saad.khurshid@ucalgary.ca

INTRODUCTION

An enthesis is the insertion of a soft tendon or ligament into stiff bone. Tendon often fail midsubstance but seldom fail at the enthesis, although the enthesis transfers load between these tissues over short distances [1]. In engineering, to transfer load between soft and stiff material safely, a long embedment distanced is required. Our objective is to study the gross morphological and collagen fibre deformation in the Achilles and the supraspinatus tendon entheses under tensile load, to understand the mechanism of load transfer. The results are compared to the previously studied medial collateral ligament (MCL) [2]. This would help us understand if the load response of every enthesis is unique.

METHODS

An Achilles or supraspinatus bone-tendon tissue complex was attached to a loading device [3] which provided tensile load while an operator tracked deformations. The enthesis area was viewed under a dual photon microscope and a stereomicroscope to study structural changes and changes in collagen fibres as tensile load was applied.

RESULTS

Six Achilles tendon samples and three supraspinatus tendon samples were used. The Achilles tendon was connected to the bone directly. Under load, the distal portion of the Achilles tendon moved closer to underlying bone as the

tendon was pulled in the direction of the load (Fig. 1). Furthermore, collagen fibres at the Achilles tendon enthesis tidemark deformed at sharp angles under load (Fig. 1). The supraspinatus tendon was connected to the bone through a large piece of fibrocartilage, and when loaded, parts of the fibrocartilage compressed. Collagen fibres in the supraspinatus tendon enthesis behaved irregularly, such as sometimes compressing or deforming at sharp angles.

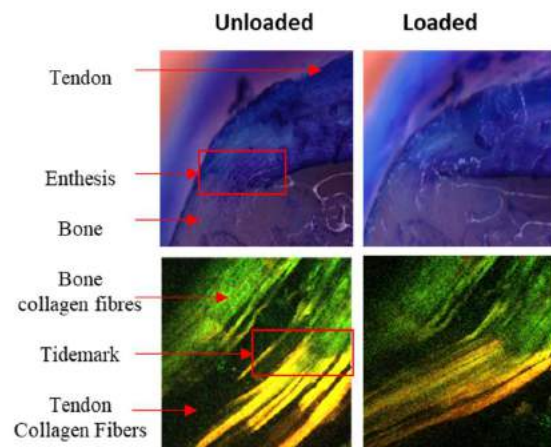


Figure 1: Top: 7x magnification picture of the Achilles tendon enthesis. Bottom: Achilles tendon collagen fibres at the tidemark. Field of View 854 um x 854 um.

DISCUSSION AND CONCLUSIONS

The response of the MCL and Achilles tendon entheses to load are similar to each other, but the supraspinatus tendon enthesis is unique. As the MCL and Achilles tendon connect to bone almost directly, fibres in the tendon were pulled in the

direction of loading, but calcified fibres in bone were static, creating a sharp angle. The supraspinatus tendon is approximately 1 cm distal to the bone connection, which creates a bending moment inside the fibrocartilage. The bending moment may cause some parts of the fibrocartilage to be under tension and some under compression, possibly leading to different results depending on the imaging location on the enthesis. In both the Achilles and supraspinatus tendon entheses, the gross morphology changes to allow the tendon to be pulled in the direction of loading. There are similarities between enthesis loaded behaviour (i.e. MCL and Achilles). However, there might be tissue-specific differences in behaviour as shown by the supraspinatus tendon enthesis. This knowledge may be helpful in designing surgical grafts.

REFERENCES

1. J. Maquirriain. *Yale J. Biol. Med.* **84**:289-300, 2011.
2. J. Sevick, M.Sc. Thesis, University of Calgary, 2017
3. M.Xu, J.Sevick, M.Chung, N.Shrive, *Journal of Undergraduate Research in Alberta*, **5**(1), 2015.



EFFECT OF ADDING ADIPOSE DERIVED MESENCHYMAL STEM CELL SECRETOME ON MIN6 PANCREATIC BETA CELL SURVIVAL

Jane Maynard¹, Jolene Phelps¹, Mark Ungrin², Arindom Sen¹

¹Pharmaceutical Production Research Facility, University of Calgary, ²Department of Veterinary Medicine, University of Calgary, jane.maynard@ucalgary.ca

INTRODUCTION

Mesenchymal stem cells (MSCs) can be found in many adult human tissues and are self-renewing and capable of differentiating into cartilage, bone, and fat-like cells. MSCs are thought to repair by differentiation into target cells and by utilization of secreted factors [1], known collectively as the secretome. The secretome contains growth factors, cytokines, and extracellular vesicles (EVs). EVs are phospholipid bilayer enclosed membranes that contain proteins and RNAs. Research has found that MSCs use paracrine signalling through the secretome as a pathway for immunomodulation and cell-to-cell communication [1]. EVs are a potential cell-free therapy and are being tested on cell models, such as MIN6 pancreatic beta cells, to evaluate their efficacy.

The purpose of this study was to evaluate the possibility of increasing proliferation and survival of the mouse derived MIN6 pancreatic beta cell line using the secretome from ethically obtained human adipose derived MSCs. This was analyzed by looking at MIN6 cell survival in the presence of the secretome.

METHODS

Pancreatic MIN6 cells were grown in healthy and diabetic streptozocin (STZ)-induced conditions in MIN6 medium. Both healthy and diabetic cells were treated with the MSC secretome supplemented medium (SSM) and MSC EVs. MSCs were grown in serum-free PPRF-msc6 medium [2]. SSM and EVs were isolated from day3

of MSC growth. SSM was obtained by centrifuging MSC expended medium in 3kDa spin filters. EVs were isolated by ultracentrifugation at 100,000 x g. SSM and EVs were re-suspended in MIN6 medium (healthy) or a 10mM concentration of STZ in MIN6 medium (diabetic). A growth curve was performed over 3 days to analyze proliferation and cell survival.

RESULTS

In comparison to the control (Figure 1a) and EV treated condition (Figure 1b), healthy MIN6 cells treated with SSM (Figure 1c) appeared to have greater cell density and aggregate formation under a light microscope. From Figure 1d, the SSM had the greatest effect on proliferation. STZ-induced diabetic MIN6 cells appeared to have similar aggregate formation and cell density in the MSC EV case and control. In the STZ condition, survival was highest in the presence of the EV fraction. curve for healthy (solid black) and STZ-induced diabetic (dotted) MIN6 cells grown in MIN6 medium (stars), MSC SSM (open circles), and MSC EVs (diamonds).

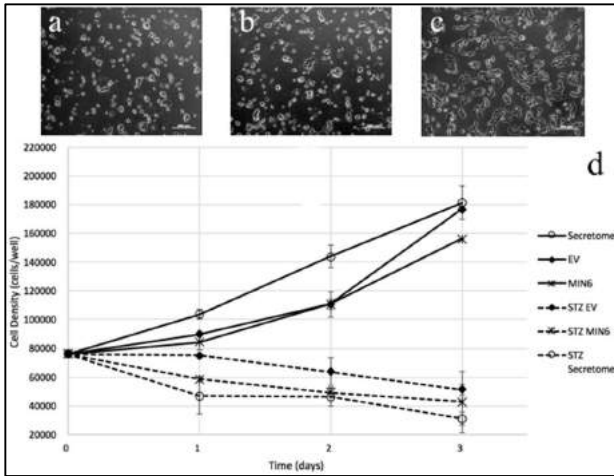


Figure 1: a) MIN6 medium b) SSM c) EV supplied medium (scale bars are 200 μ m) d) 3-day growth

DISCUSSION AND CONCLUSIONS

Adipose derived MSC SSM may have a proliferative effect on healthy MIN6 cells. There is an increase in aggregation and growth for healthy MIN6 cells in SSM. The SSM may contain cell signalling factors that encourage MIN6 cell growth. EVs may help decrease STZ-related death on MIN6 cells. EV supplied medium appeared to have the highest survival rate in the presence of STZ. MSC EVs potentially contain cargo that aids MIN6 cell survival in an induced diabetic cell model. In the future, different concentrations and time points of collection of EVs and SSM will be tested.

REFERENCES

1. Sarvar et al. *Adv Pharm Bull.* **6(3)**:293-299, 2016.
2. Jung et al. *J Tissue Eng Regen Med.* **6**:391-403, 2012.



HIGH-FAT, HIGH-SUCROSE DIET AND YOUNG RAT MUSCLE FUNCTION

Curtis A. Ostertag¹, Ian C. Smith¹, Graham Z. MacDonald¹, Walter Herzog¹

¹Human Performance Lab, Department of Kinesiology, University of Calgary
costertag18@gmail.com

INTRODUCTION

Muscle strength is among the most important factors determining one's ability to carry out activities of daily living. On average, the muscles of people with obesity produce less force per unit body mass [1] and less force per unit muscle volume [2] than the muscles of people without obesity. This impairment in muscle function may result from less contractile tissue caused by fibrosis or intramuscular fat infiltration [1], or through dysfunction of the contractile proteins themselves. Examining how obesity affects muscle contractile function at the cellular level would be helpful in determining the link between muscle weakness and obesity. The aim of this study was to determine how a high-fat, high-sucrose (HFS) diet affects the contractile function of single permeabilized rat muscle fibres isolated from young animals. Maximum stress production (force produced per cross-sectional area) and maximum rate of shortening (fibre lengths per second, V_0) were used as indicators of muscle contractile function, and we hypothesised that both measures would be impaired in the HFS group relative to the control group of normal chow-fed rats.

METHODS

Beginning at 3 weeks of age, age-matched rats were randomly assigned to either a normal chow diet (Chow; 12% fat, 0% sucrose; $n=4$), or a HFS diet (40% fat, 45% sucrose; $n=4$). After 14 weeks on the diets, body composition of the rats was assessed using dual-energy x-ray absorptiometry (DXA) and the vastus intermedius (VI) muscles

were harvested and chemically skinned. Contractile function was tested at 19°C. Maximum stress production was measured in fully activated fibres using a solution of excess calcium (pCa 4.2). Fibres were designated as slow or fast based on their sensitivity to strontium at pSr 5.0. The number of fibres assessed in each group were: Chow Slow-14, Chow Fast-19, HFS Slow-16, and HFS Fast-17. V_0 was assessed in each fibre by the slack test method [3] with fully active fibres being rapidly shortened by 14-17% of total fibre length and the slack time measured. Body composition data were analyzed using a Student's t-test. Contractile data were analyzed using a 2-way factorial ANOVA, with fibre type and diet as independent variables. An α of 0.05 was taken as significant.

RESULTS

DXA scans showed that the HFS rats had higher ($P<0.05$) fat mass (HFS: 177.9 ± 10.3 g vs Chow: 79.2 ± 5.2 g), total mass (HFS: 653 ± 17 g vs Chow: 548 ± 17 g), and body fat percentage (HFS: 27.2 ± 4.0 % vs Chow: 14.4 ± 2.3 %). There was no difference in lean mass + bone mineral content (HFS: 475 ± 13 g vs Chow: 469 ± 15 g). We saw no differences between the two diet groups in either maximum stress production or maximum rate of shortening (Figure 1). Fibre type differences were detected for V_0 but not for maximum stress.

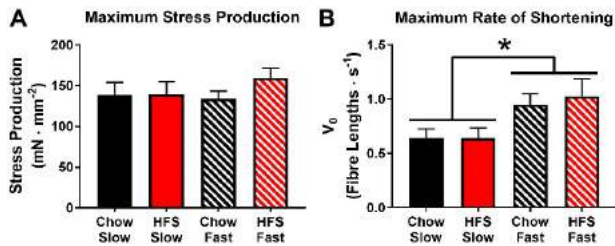


Figure 1: Contractile function of chemically permeabilized fibres. **A:** Maximum stress production in each group of fibres. **B:** Maximum rate of muscle shortening (V_0) in each group of fibres. *- Fast fibres \neq Slow fibres; $P < 0.05$.

DISCUSSION AND CONCLUSIONS

The results of our tests show that while the HFS rats had approximately twice as much body fat as the Chow group, the HFS diet did not affect either maximum stress production or V_0 in the vastus intermedius fibres of the young male rats. Even though these findings refute our hypothesis, they suggest that the contractile proteins are functioning properly, despite the increase in body fat content. Rats of different ages, female rats, and rats exposed to a longer HFS diet may be affected differently than the cohort of rats used in our study. It is also unclear how obesity affects the contractile function of human muscle proteins. Future studies must take these remaining questions into consideration.

REFERENCES

1. Tomlinson et al. (2016) *Biogerontol* 17:467-483
2. Tomlinson et al. (2014) *Physiol Rep.* 2(6):e12030
3. Reggiani. (2007) *J Physiol.* 583(1):5-7



Chuckwagon Pole Design and Material Behavior

Sam Pollock¹, Renaud Léguillette^{2, 3}, Art Kuo^{2, 4}, Mark Ungrin^{2, 3}

¹Schulich School of Engineering, University of Calgary, ²Biomedical Engineering Graduate Program, University of Calgary, ³Faculty of Veterinary Medicine, University of Calgary, ⁴Faculty of Kinesiology, University of Calgary
pollocks@ucalgary.ca

INTRODUCTION

Chuckwagon racing is an equine racing sport that has been an event at the Calgary Stampede since 1923 [1]. Accidents during chuckwagon races, have caused injuries and fatalities to both horses and drivers [1]. A chuckwagon pole is the metal poles that extends from the front of a wagon and serves as an attachment point for the four horses. The pole is a key element for force transmission and experiences both tensile force and a bending moment during racing, as the wagon completes its turn around the top barrel. Anecdotal evidence from experienced chuckwagon drivers and Nelson (1993) indicate that accidents due to pole breakage have occurred, although specific data such as incidence rates have not been collected. The aim of this collaborative Faculty of Veterinary Medicine/Biomedical Engineering project was to study the design and material behaviour of chuckwagon poles to better understand chuckwagon racing safety.

METHODS

Qualitative and quantitative methods were used to conduct the research. The 36 chuckwagon drivers competing at the 2017 Calgary Stampede were interviewed and surveyed to identify existing pole designs and explore drivers' opinions on pole design. Each pole's length, diameter and thickness were then measured to determine physical dimensions. GoPro cameras were used during training and racing to digitally record video of pole behavior. Acceleration and angular acceleration of the front and rear of poles was measured by inertial

measurement units and used to indirectly calculate pole deformation.

Axial and bending strain were measured on poles using three uniaxial strain gauges in a 350 Ω quarter bridge configuration.

Compression testing was used to determine the ultimate strength of a sample of pipe.

RESULTS

Of the 36 poles used at the 2017 Calgary Stampede, there were 14 different designs made of at least five different types of steel. Six of the 36 competing drivers had previously broken a pole during a competition. Figure 1 depicts pole service life. The median outside diameter and thickness of the poles were 2.75 in. (IQR: 0.25) and 0.125 in. (IQR: 0), respectively. The mean maximum strain measured during racing was 1076 μ mm/mm.

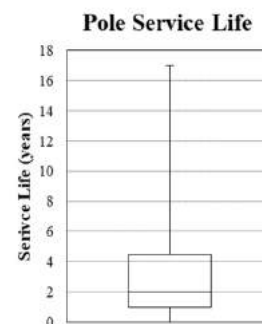


Figure 1: Service lives of the chuckwagon poles used at the 2017 Calgary Stampede, as reported by drivers. The median service life was two years (IQR: 3.9 years). The maximum service life was 17 years.

DISCUSSION AND CONCLUSIONS

Analysis of the strain data, along with qualitative analysis of the GoPro video, indicates that although poles bend during racing, normal racing conditions are unlikely to cause plastic deformations. Survey results indicated that several drivers are using poles that have exceeded the median expected service life of the average pole. These poles may be at risk of failure due to fatigue.

In summary, there is variety in the design, material, and construction of chuckwagon poles. Chuckwagon racing places highly variable forces on poles. More research into the design and behavior of chuckwagon poles is recommended.

REFERENCES

1. Doug Nelson. *Hot Cakes to High Stakes: The Chuckwagon Story*. 1993.



RUNNING UP WALLS: THE DYNAMICS OF LEG FUNCTION IN A PARKOUR WALL CLIMB

Fatima Saleem¹, Musab Shams¹, Ryan Schroeder¹

¹Center for Mobility and Joint Health, University of Calgary, fatimas17@educbe.ca

INTRODUCTION

Parkour is an extreme sport that pushes the functional limits of the human body. In the wall climb task, the goal is to abruptly transition from a horizontal to a vertical trajectory [1]. This study aims to understand the motor control task of navigating such an unusual circumstance. By studying the human system as it approaches performance limits, the underlying control mechanisms are likely to become more apparent. Although Parkour is an unusual activity, traditional biomechanics techniques can still be used to analyze effective leg operation and other movement strategies [1, 2].

The purpose of the study is to use the wall run as a model that illuminates fundamental objectives of more generalized human locomotion as a physiological task in a boundary-pushing physical environment.

METHODS

Six Parkour enthusiasts, with varying weights and heights, were recruited from Perth Parkour in Western Australia. Each subject performed approximately ten to fifteen trials, attempting to climb a three-meter wall. The athletes had ample space to perform a run-up and climb the wall. Two force plates were used to measure ground reaction forces – one on the ground and one on the wall. Data for the run were excluded if the individual did not make contact with the two force plates.

Video data was collected from a GoPro Hero to capture the sagittal plane view. One marker was

placed at a lower lumbar position, approximately at the center of mass. Additionally, two markers were placed on each foot, one near the heel and one near the toe. These markers were tracked in a custom MATLAB (R2016a) program [1]. The participant's center of mass kinematics were determined in two ways: using force-plate measurements and initial conditions captured from the video. These two methods were compared for validation.

RESULTS

Trajectory data calculated from both the force plates and the video were qualitatively similar between the different subjects verifying that appropriate initial conditions were identified (Figure 1). The variation in the video data and the force plate data that can be seen towards the right of the graph is due to the change in the position of the limbs relative to the trunk, which alters the center of mass position (Figure 1).

Average magnitude of the vertical reaction force was larger for the ground plate, while the vertical reaction forces hardly exceeded bodyweight on the wall plate. Upward velocity increased during ground contact, decreased during no contact, and was maintained near a constant value during wall contact.

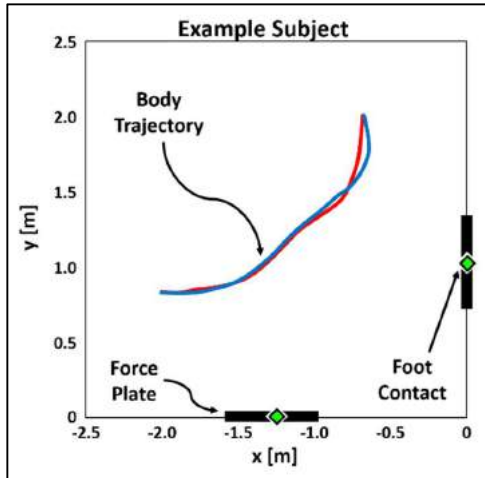


Figure 1: A plot of the body trajectory from lateral view, comparing the video data (red) and the force plate data (blue) for a single individual.

REFERENCES

1. Lawson, P. *Undergrad. Honors Theses*. Paper 879.
2. Maulder P. & Puddle, D. *J Sport Sci Med*. 1(12), 122-129, 2014.
3. Hedrick T.L. *Bioinsp. And Biomim*. **3**: 034001, 2008.

DISCUSSION AND CONCLUSIONS

Future analyses will focus on comparing unsuccessful with successful trials – to determine the key features of movement patterns that differentiate between the two. This will not only allow for the understanding of the physical task, but also how it integrates with the neural and physiological function.



Blood Flow and Nanoparticle Distribution in Zebrafish Blood Vessels

Branden Shin¹, Juliana Gomez², Hagar Labouta^{2,5}, Bahareh Vadafar³, Sarah J. Childs⁶, Kristina D. Rinker^{2,4,7}

¹Biomedical Engineering Program, UofC, ²Cellular and Molecular Bioengineering Research Lab, ³Zymetrix Lab, ⁴Department of Chemical and Petroleum Engineering, ⁵Department of Chemistry, ⁶Department of Biochemistry and Molecular Biology, ⁷Center for Bioengineering Research and Education
branden.shin@ucalgary.ca

INTRODUCTION

Medical nanoparticles have emerged as a powerful tool for both drug delivery, and diagnostic techniques [1]. These particles are roughly 100nm in diameter and are injected into the bloodstream where they target the blood vessel walls. However, it is important to understand how factors such as blood flow or vascular architecture affect their distribution.

After injection into the bloodstream, nanoparticles will target the cells lining the blood vessel wall called the endothelial cells (EC's). Because the EC's are exposed to fluid flow, they experience fluid forces such as wall shear stress. Previous *in vitro* studies have determined that the distribution of nanoparticles is related to the wall shear stress, where areas of lower shear stress result in higher levels of nanoparticle accumulation [2,3,4]. Our group explored the effects of vascular flow on nanoparticle distribution *in vivo* for the first-time using carboxylate-coated nanoparticles [3]. This study intends to explore the effects of vascular flow on a different nanoparticle, now using liposomes.

METHODS

Transgenic zebrafish embryos are chosen as they are optically transparent. The EC's express a green fluorescence, and the red blood cells are red. A three-dimensional (3D) geometry of the

vasculature is generated by collecting confocal images from zebrafish embryo and importing them into the 3D imaging software Simpleware ScanIP Version 4.3. Line scans were collected along the centreline of each vessel of interest, and particle image velocimetry of the red blood cells was performed by Bahareh Vadafar in the Zymetrix Lab to calculate the average velocity of the blood flow. The vessels to be examined are the dorsal aorta, and the vessels that make what is known as the caudal venous plexus: the dorsal vein, ventral vein, and capillaries. These are chosen as the dorsal aorta is characterized by straight blood vessels, whereas the venous plexus is composed of disturbed flow patterns, which allows us to investigate the effects of vascular architecture on nanoparticles.

RESULTS

The average blood flow velocities are $497.96 \pm 290.64 \mu\text{m/s}$ in the dorsal aorta, and $246.25 \pm 148.25 \mu\text{m/s}$ in the ventral vein. The nanoparticle accumulation per unit volume (μm^3) relative to that in the capillaries were determined to be 0.122 ± 0.052 for the dorsal aorta, 0.336 ± 0.240 for the ventral vein, 0.691 ± 0.468 for the dorsal vein, and 1.0 for the capillaries. The results showed nanoparticles localized in areas of disturbed blood flow. Additionally, the blood flow velocity affected nanoparticle accumulation, as the faster blood flow

vessels contained less nanoparticles, because the blood pushes the nanoparticles away from the blood vessel wall.

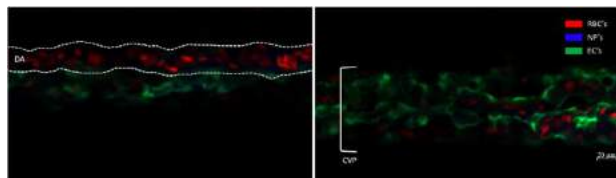


Figure 1: The figure above shows confocal images of the dorsal aorta (left) and the caudal venous plexus (right) of the zebrafish embryo. The nanoparticle signal has a higher intensity in the plexus, indicating a higher accumulation in that region.

DISCUSSION AND CONCLUSIONS

The results showed that blood flow and vascular architecture play a significant impact on the distribution of nanoparticles in the bloodstream of the zebrafish embryos. The liposomes accumulated in areas of lower shear stress and altered architecture, showing that blood flow has an effect on nanoparticle distribution. In order to optimize medical nanoparticles for treatment or diagnostic techniques, we must understand the behaviour of such particles in the presence of blood flow.

REFERENCES

- [1] Murthy, *Int J Nanomedicine*. **2**: 129-141, 2007.
- [2] Jiang et al. *Nanomedicine*. **13**: 999-1010, 2017.
- [3] Gomez et al. *Small*. In Submission
- [4] Sarsons et al. *J Biomed Nanotechnol*. **10**: 1641-1676



GEOMETRIC AND STRAIN-BASED ANALYSIS OF ABDOMINAL AORTIC ANEURYSMS UNDERGOING OPEN REPAIR VS ENDOVASCULAR REPAIR

Harsupreet Sidhu¹, Flavio Bellacosa Marotti¹, Arianna Forneris², Randy Moore³, Elena S. di Martino¹

¹Biological Tissue Mechanics Lab, University of Calgary, ²Biomedical Engineering Program, University of Calgary,

³Department of Surgery, University of Calgary, harsupreet.sidhu@ucalgary.ca

INTRODUCTION

Abdominal aortic aneurysms (AAAs), which account for 80% of aortic aneurysms, occur between the renal arteries and aortic bifurcation, below the chest. Patients who have ruptured AAAs only have a 50% chance of reaching the hospital alive, and then only up to a 50% chance of survival after surgery [1]. Currently, there are two treatment options: open repair surgery, which is completed by making a large incision or endovascular repair, which only requires a small cut for insertion of an endograft [1].

Our lab currently investigates the mechanical properties of the aorta of AAA patients to determine if it may provide indications to surgeons to determine if a patient should be considered for open repair surgery. The type of surgery a patient undergoes is normally decided based on clinical and geometrical factors including proximal neck angulation, diameter of the iliac artery, and certain patient features such as age and gender [1,2]. The aim of this project was to determine if intraluminal thrombus thickness and local deformation of the aortic wall, obtained pre-operatively, can be used to determine which AAAs should be selected for open repair surgery.

METHODS

Ten male patients ranging from age 67 to 80 undergoing surgical repair of their AAAs at Peter

Lougheed Hospital, 5 undergoing open surgery and 5 endovascular surgery, were selected and analyzed. Through a series of steps, we obtained a final set of averaged data different locations on the aorta for the thickness of intraluminal thrombus the following mechanical properties: maximum principal stress, maximum principal strain and the constrained deformation ratio (CDR), a ratio of circumferential and axial stretch. Key steps included acquiring multiphase CT images and creating a 3D reconstruction of the aorta that was split into patches giving us a total of 48 data measurements for each patient. One-tailed t-tests for comparison between operation types and two-way analysis of variance (ANOVA) using patients and patches as factors were run to observe statistically significant differences ($p < 0.05$).

RESULTS

There is an observable difference in thrombus thickness between the two groups, as seen in Figure 1. The two-way ANOVA showed significant difference among individual patients for both maximum principal strain and CDR, and between patches for CDR. However, the statistical differences for the mechanical properties were not significant when comparing between each surgery type.

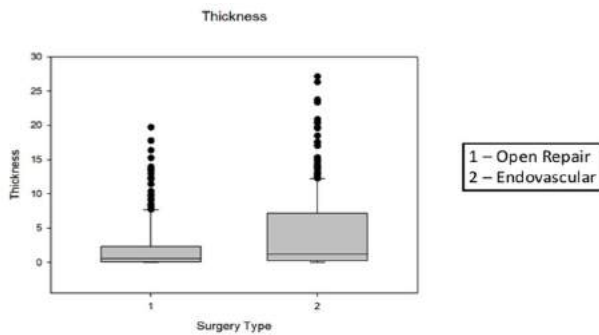


Figure 1: A boxplot representing the thrombus thickness in patients of each population shows that group 2 has greater variation.

DISCUSSION AND CONCLUSIONS

The absence of any statistical difference in the mechanical properties (strain and stress measures) between the two groups suggests they are not factors in determining which operation a patient should undergo. The results from thrombus thickness showed that patients selected to undergo endovascular repair had more variation in thicknesses and an overall greater mean. Looking at differences among patients and using the location on the aorta as a factor, we found that the maximum principal strain was different between patients, suggesting that strain measures can be used to classify patient risk. CDR was different between patients and based on the location on the aneurysm. CDR may be especially interesting since the areas on the aortas where this property was consistently elevated corresponded with areas deemed as high risk of rupture by surgeons.

REFERENCES

1. Aggarwal et al. *Exp Clin Cardiol.* **16**:11-15, 2011.
2. Iezzi & Cotroneo. *Abdom Imaging.* **31**:722-731, 2011.



IMPLEMENTING CHEMO-OPTICAL PROCEDURES IN A UNIQUE COUPLED OPTICO-MECHANICAL MINI- BIAXIAL EXPERIMENT FOR A DEEPER INSIGHT INTO MICROSTRUCTURE OF DEFORMED TISSUE

Donovan Stagg^{1,4}, Youssef Beauferris^{2,4}, Taisiya Sigaeva^{2,3}, Elena Di Martino^{3,4}

¹Chemical Engineering, University of Calgary, ²Mechanical Engineering, University of Calgary, ³Civil Engineering, University of Calgary, ⁴Biomedical Engineering Specialization, University of Calgary, donovan.stagg@ucalgary.ca

INTRODUCTION

Biaxial tensile testing is a common technique used to fully characterize the inherent anisotropic properties of soft tissues [1]. These properties can be further used in advanced models to study or predict various biomechanical phenomena. However, understanding the microstructural properties of soft biological tissues, such as the behaviour at the cellular level or behaviour of its microstructures such as collagen and elastin [2], can significantly increase the accuracy of biomechanical models. The research objective was to couple confocal imaging and biaxial mechanical testing of soft biological tissues. Imaging tissue sample nuclei can be used to calculate localized deformations of the sample, and imaging collagen fiber undulation will help to determine ranges of deformation at which collagen or elastin contributions are dominant.

METHODS

To allow for the coupling of a biaxial tensile test with confocal microscopy imaging, a miniaturized version of a conventional biaxial machine (mini-biaxial machine) was utilized. A Fluoview FV1000 confocal laser scanning microscope was used to perform fluorescence and confocal imaging. Both normal porcine and pathological aneurysm human ascending aortic samples (7mm x 7mm x 1.5mm,

unfixed) were stained with Hoechst 33258 nuclear stain to stain nuclei, and with picrosirius red stain (Direct Red 80 in picric acid) to stain collagen filaments. Stained samples loaded into the mini-biaxial machine were fitted under the confocal microscope to image while undergoing a modified 30% strain biaxial tensile test, where the test was paused, and the sample imaged after every 5% displacement. Unstained, formalin-fixed samples were also imaged with a dual-photon microscope to view collagen and elastin structure.

RESULTS

The mini-biaxial machine was successfully fitted under the confocal microscope, and a biaxial test was run on tissue samples without interference from the microscope itself. Tissue samples stained with Hoechst 33258 nuclear stain were successfully imaged during the modified 30% strain test, which allowed tracking of the displacement of sample nuclei throughout the test. Imaging picrosirius red stained samples was less successful due to difficulties staining large samples, as no distinct collagen microstructures could be identified. Dual-photon microscopy of fixed samples yielded clear images of both collagen and elastin.



Figure 1: Left - coupled mini-biaxial machine and confocal microscope system. Right - confocally imaged porcine aorta sample with stained nuclei midway through modified biaxial test.

DISCUSSION AND CONCLUSIONS

A confocal laser scanning microscope and a mini-biaxial machine were successfully coupled in an optico-mechanical system, allowing simultaneous mechanical testing and laser confocal imaging of samples. Displacements of sample nuclei during a biaxial test were imaged and tracked, and analysis can be performed on these images to identify the sample's local mechanical properties. Sample collagen microstructures could not be clearly imaged, due to the large size of the tissue samples and improper staining protocol. Further experimentation with picosirius red staining techniques is necessary before the collagen filament undulation can be observed. Dual-photon imaging may be a preferable alternative for viewing microstructure behaviour. Overall, the optico-mechanical coupling of a mini-biaxial machine and a confocal microscope is promising and will allow us to better understand the behaviour of tissue microstructures during a biaxial tensile test.

REFERENCES

1. Lanir & Fung. *J. Biomechanics*. 7:171-182, 1974
2. Patel et al. *Cardiovascular Research*. 71:40-49, 2006



ENERGY OPTIMIZATION RESURRECTS EXTINCT MAMMAL LOCOMOTION

Jena Whiteside¹, Delyle T Polet², John EA Bertram³

¹Faculty of Science, University of Calgary, ²Department of Biological Sciences, University of Calgary,

³Cumming School of Medicine, University of Calgary, jena.whiteside1@ucalgary.ca

INTRODUCTION

While fossil trackways can be valuable tools in divulging the locomotion of early mammals, associating track data with a species or genus can be a challenge. This issue is exemplified by a camelid trackway discovered in Bear Springs, Arizona [1]. Based on stride length and footprint morphology, the track maker could only be broadly inferred as either *Pleiolama vera* or a member of the genus *Hemiauchenia*.

This study's objective was to test if a neglected measurement – spacing between individual footfalls – could help identify an ambiguous track maker with a higher degree of precision. Since organisms tend to move in a manner that minimizes energy cost, the different morphologies of different species lead to unique locomotive patterns that maximize efficiency. By extension, if it were possible to model energy use as a function of morphology, it is feasible that this problem could be solved by generating model footfall patterns for different inputted morphologies. In doing so, it is hypothesized that candidate footfalls could be compared to the initial trackway to pose a more precise estimate as to the actual track maker.

METHODS

To simulate energy optimization, the quadrupedal optimal control model described by Polet et al. [2] was used. It required five inputs: speed, forequarter mass, and forelimb, hindlimb, and stride lengths. Masses and lengths were normalized to body mass and torso length, respectively.

Morphological data from the literature was compiled for four candidate species, chosen to reflect a broad range of possible body sizes within the *Hemiauchenia* genus (*P. vera*, as noted, was already identified to species). To fill in missing data, regression equations for relative limb bone lengths were used, while relative stride length and Froude number (stride length and speed normalizations) were found via regressions from Alexander and Jayes [3]. All values were then inputted.

RESULTS

For each candidate species, root mean squared error (method of representing standard deviation of discrepancies between predicted/observed values) was used to quantify the spacing discrepancies between the mystery trackway and computer-generated footfall patterns (Figure 1). With minimal deviation, *H. macrocephala* appears to be the most probable track maker. *H. paradoxa* is close behind, whereas *H. gracilis* and *P. vera* manifest as the least likely candidates.

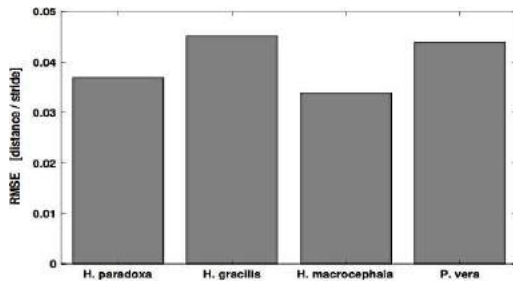


Figure 1: A comparison of the discrepancy between print placement on the mystery trackway and computer models. The y-axis shows RMSE (distance/stride; dimensionless); the x-axis shows species.

DISCUSSION AND CONCLUSIONS

Supporting the hypothesis, the results of this study suggest that when the locomotor implications of energy optimization are considered, analyzing spacing between footfalls improves precision in species identification from trackways. While the initial predictions regarding the Bear Springs trackway failed to discriminate between two genera, this energy optimization model enables researchers to evaluate the probability of a trackway belonging to a particular species. However, for this particular study, the small differences in RMSE across all candidates hinder conclusive track maker identification.

REFERENCES

1. Thompson et al. *Cenozoic Vertebrate Tracks & Traces*. 309-314, 2007.
2. Polet et al. "Optimal control describes quadrupedal walking in dogs." *Dynamic Walking*. June 4-9, 2017; Mariehamn, Finland.
3. Alexander & Jayes. *J. Zool.* **201**:135-152, 1983.



THE MECHANICS OF AGONIST MUSCLES

Kalvin Wu¹, Seong-won Han², Andrew Sawatsky², Heiliane de Brito Fontana³,
Walter Herzog²

¹Biomedical Engineering Program, University of Calgary, ²Faculty of Kinesiology, University of Calgary, ³Department of Morphological Sciences, Federal University of Santa Catarina, Brazil, wherzog@ucalgary.ca

INTRODUCTION

A widely used assumption in musculoskeletal biomechanics is that the sum of individual muscle torques are equal to the torque produced when all muscles are contracted simultaneously. However, previous observations found that the sum of individual muscle torques was greater than the torque produced by a simultaneous contraction of all the muscles [1]. Two speculations on the cause of this torque difference have been suggested: i) that force is transmitted transversely (laterally) through the connective tissue in agonist muscle groups [4], or ii) that the patellar moment arm length varies with the muscle being stimulated.

The purpose of this study was to investigate whether the loss of torque in simultaneous versus individual muscle activation in the quadriceps group is the result of either lateral force transmission or a changing patellar moment arm length.

METHODS

Surgery was performed on the right hind leg of New Zealand white rabbits (n=2) to expose the individual nerves of the vastus lateralis, rectus femoris and vastus medialis. Nerve cuffs were used to provide electrical stimulation and a voltage 2.5 times greater than the threshold voltage was applied, ranging from 4-6V. Testing was done at various knee joint angles (40-120 degrees while 0 degrees was fully extended) and trials were performed before and after a blunt dissection of the connections between the target muscles to eliminate lateral force transmission between these

muscles.

In this study, both the knee extensor torque and muscle forces were measured. The torques were measured using a load cell at the end of the tibia, while muscle forces were measured by inserting an implantable force transducer (IFT) inside the patella ligament [2,3]. Unlike the torque, force values measured from the IFT are independent of the patellar moment arm length.

RESULTS

The sum of individual torques was greater than the torque generated by a simultaneous contraction for all knee joint angles both before (PRE) and after (POST) isolation of muscles (Figure 1). This suggests that lateral force transmission was not the cause of this torque difference. Similarly, the sum of individual forces measured using the IFT was greater than the force generated by simultaneous muscle contraction (Figure 1). This suggests that possible moment arm length changes were also not the cause of the torque difference.

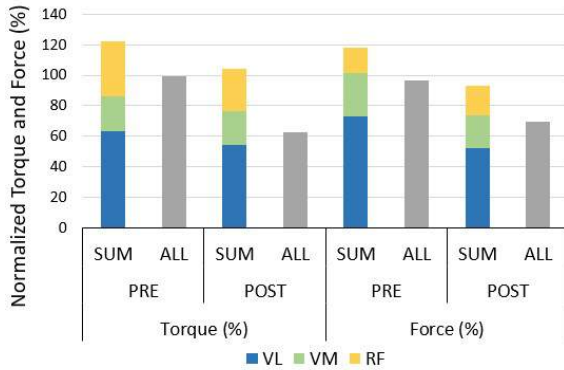


Figure 1: Representative result obtained at one knee joint angle (90 degrees). 100% of muscle torque/force was defined as the maximum value when all muscles were activated simultaneously. Sum of individual muscle torques/forces (SUM) and muscle torques/forces of a simultaneous contraction (ALL) are shown before (PRE) and after (POST) isolation of muscles.

DISCUSSION AND CONCLUSIONS

The loss of torque was not the result of either lateral force transmission or a changing patellar moment arm.

REFERENCES

1. de Brito Fontana H. et al., *J Biomech.* (Submitted, 2017)
2. Herzog, W., Archambault, J. M., Leonard, T. R., Nguyen, H. K., (1996). Evaluation of the implantable force transducer for chronic tendon-force recordings. *Journal of Biomechanics* 29, 103-109.
3. Herzog, W., Hasler, E. M., Leonard, T. R., (1996). In-situ calibration of the implantable force transducer. *Journal of Biomechanics* 29, 1649-1652.
4. Mass & Sandercock. *J Biomed Biotechnol.* 2010:575672, 2010.



Advancing a Novel Coupled Optico-Mechanical Mini-Biaxial Device

Youssef Beauferris, Donovan Stagg, Taisiya Sigaeva, Elena Di Martino

¹Biological Tissue Mechanicals Lab, University of Calgary, ²Biomedical Engineering Program, University of Calgary, youssefbeauferris@ucalgary.ca

INTRODUCTION

Biaxial Testing is a useful method for studying the mechanical characteristics of anisotropic materials such as soft tissues. Knowing these characteristics is useful when trying to predict the behaviour of pathological and healthy soft tissues in the body. The Bose Electroforce Planar Biaxial Test Bench at the University of Calgary (Zymetrix) has proven to be reliable in deriving accurate data for soft tissues, but is lacking in portability and is hard to integrate with an optical microscope. The Cardiovascular Mechanics Lab has recently developed a miniaturized biaxial device coupled with a confocal microscope. The first objective of this study is to test the reliability of the miniature biaxial device in comparison to standard biaxial devices. The second is to observe the microstructure of deformed soft tissues using the confocal microscope, and to assess the viability of tracking nuclei displacement for local measurements. We do this using staining procedures which allow for the observation of nuclei, collagen and elastin. Doing so would offer an alternative to current local measurement methods and give us more insight into the tissue's behavior.

METHODS

The mini-biaxial was used to test small samples (6 x 6 mm) of pathological (aortic aneurysm) and healthy soft tissues. Hooks were used to secure the sample and attach them to the arms which induce deformation. Six displacement protocols were

created with differing values of stretch ratio for each axis, duration and number of stretch cycles, and the waveform of stretch cycles. Three dots were drawn on the face of each sample in a triangular pattern allowing for collection of local data via custom camera setup. Global loads (Hook), and local displacements (Dots) were recorded and analyzed through Matlab to obtain stress vs. strain curves. Plane stress and strain were assumed in the analysis. Samples of healthy pig aorta were tested and compared on the newly developed mini-biaxial machine and the conventional Bose Electroforce Planar Biaxial Test Bench. The images obtained using Hoechst were compiled in series in attempt to track nuclei displacements.

RESULTS

Global load measurements collected from testing healthy pig aorta on the mini-biaxial (Figure 1c) were compared to global load measurements obtained using the large biaxial (Figure 1b). The resulting stress vs. strain curves demonstrated remarkable similarity in magnitude, and both exhibited non-linear profiles. Local measurements collected from testing a sample from the same healthy pig aorta on the large biaxial were also analyzed. The resulting curve followed a similar non-linear profile to the results of the mini-biaxial.

Microscope images were successfully obtained from a human aortic aneurysm. A series of images were collected in 5% strain increments. Images

were also successfully obtained using the picrosirius red stain.

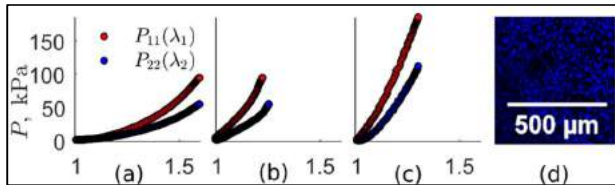


Figure 1: (a) Bose test bench global analysis (b) Bose test bench local analysis (c) Mini-biaxial global analysis (d) Image collected from aortic sample using Hoescht nuclear stain

DISCUSSION AND CONCLUSIONS

Comparing the global results from the mini-biaxial to the local results from the large biaxial it is apparent that they measure similar non-linear curves. It can be concluded that the mini-biaxial provides reliable data that is similar to a commercially developed biaxial device.

Nuclei from Hoescht images could potentially replace the use of dots for local data collection. However, when compiled the clusters that are tracked seem to maintain the same distance between one another. This may be a result of testing tissues which have thawed. As a result, cells inside the tissue may have burst meaning the clusters observed may not be nuclei. Further research must be conducted in order to assess the viability of local data collection through optico-mechanical coupling.



SARCOMERE OPERATING LENGTHS OF FROG LEG MUSCLES

Carissa Chung¹, Venus Joumaa², Andrew Sawatsky², Walter Herzog^{1,2}

¹Biomedical Engineering Program, University of Calgary, ²Human Performance Lab, University of Calgary, cmychung@ucalgary.ca

INTRODUCTION

Frogs show outstanding skeletal muscle performance when jumping and swimming. Understanding the origin of this performance would provide great insight into muscle function and thus help us advance our approaches in muscle tissue engineering. Muscle produces active and passive forces. Active forces are produced when the muscle is electrically stimulated and energy is used to shorten and lengthen the muscles during concentric and eccentric contractions, respectively. Passive forces are produced as the muscle is lengthened without activation and without energy cost. The active and passive forces depend on sarcomere lengths (SLs) [1]. At short SLs, active force is minimal; as SLs increase, active forces increase until they reach a plateau and then decrease as SLs further increase. Passive forces increase as SLs increase [1]. In order to better understand the outstanding muscle performance in frogs, it is necessary to characterise the SLs at which muscles operate *in vivo*. If muscles operate at SLs that favor the production of passive forces, then the energy cost of force production is reduced, and muscle efficiency and performance are greatly enhanced.

Our purpose was to investigate the operating SLs of three frog leg muscles throughout the physiological range of ankle motion using two methods of analysis, laser diffraction and phase-contrast light microscopy. We hypothesized that frog leg muscles operate at SLs that would favor

passive force production and thus reduce the energy cost of movement.

METHODS

Ten frog legs were fixed at a knee angle of 5 degrees and different ankle angles of 20, 35, 50, 65, 80, 95, 110, 125, 140, and 155 degrees of dorsiflexion. The tibialis anterior, gastrocnemius, and peroneus muscles were isolated using surgical techniques and digested in 30% nitric acid for ten hours to allow for the isolation of muscle fiber bundles. Five fibre bundles were isolated from each muscle and placed onto glass microscope slides and their average SLs were determined using laser diffraction and phase-contrast light microscopy.

Laser Diffraction: Laser light was shone through the fibers on the slides and the distances between the first and zero order diffraction lines were measured and converted to SLs.

Microscopy: Slides were imaged at 40x objective using a phase-contrast microscope. MATLAB was used to place markers along the myofibrils to determine SLs.

RESULTS

The gastrocnemius muscle showed a decrease in SLs from 2.1 to 1.5 μm as the ankle angle increased from 20 to 155 degrees of dorsiflexion (Figure 1). The SLs in the tibialis anterior increased from 2.2 to 3.3 μm as the ankle angle increased. The peroneus showed SLs within the range of 2.0 to 2.2 μm . Similar results were obtained using the phase-

contrast microscope thereby confirming results obtained using laser diffraction.

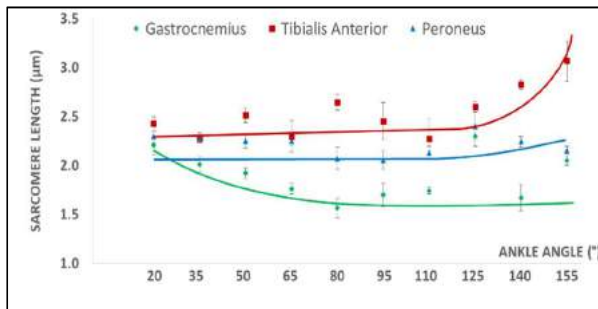


Figure 1: Sarcomere lengths as a function of ankle angle from laser diffraction. Error bars represent standard deviations of sarcomere length values ($n = 20$) for each muscle at a different ankle angle.

DISCUSSION AND CONCLUSIONS

The tibialis anterior muscle operates at noticeably long SLs compared to the gastrocnemius and peroneus muscles. Knowing that passive force increases as the SL increases, this finding suggests that the tibialis anterior muscle produces large passive forces as the ankle angle extends. This large passive force would have beneficial implications for the muscle function during everyday activities, as it would allow frogs to flex their feet passively using the elastic recoil forces of the tibialis anterior without muscle activations. This could decrease the energy cost of swimming and jumping and explain why frogs are able to perform so efficiently in these tasks. Future research should involve measuring EMG activity in the frog leg muscles during swimming and jumping to test this hypothesis.

REFERENCES

1. Gordon AM, *et al.* *J Physiol.* **184**(1):143-169, 1966.



The Effect of Enzyme Type and Agitation Rate and Regime on the Harvest of Equine Cord Blood Mesenchymal Stem Cells from Microcarriers

Tiffany Dang¹, Erin Roberts^{1,3}, Thomas G Koch⁴, and Michael S. Kallos^{1,2,3}

¹Pharmaceutical Production Research Facility, ²Department of Chemical and Petroleum Engineering, Schulich School of Engineering, ³Biomedical Engineering Graduate Program, University of Calgary,

⁴Department of Biomedical Sciences, Ontario Veterinary College, University of Guelph, Gordon St. N1G 2W1, Guelph, Ontario, Canada

tiffany.dang@ucalgary.ca

INTRODUCTION

Musculoskeletal injuries are the leading causes of lameness and loss of performance in horses. [1] Although conventional treatments exist, they often require long recovery times and result in high rates of re-injury. One potential treatment is the use of equine cord-blood derived mesenchymal stem cells (eCB-MSCs) due to their high proliferative capacity, immunomodulatory properties and chondrogenic potential. [2] The potential of these cells is currently hampered by the inability to grow them in quantities required for multicenter clinical studies and commercial product development. However, culturing the cells on microcarrier beads in stirred suspension bioreactors, allows for extensive cell expansion. Despite existing protocols in the literature for the removal of mesenchymal stem cells from microcarriers, exist for the removal of eCB-MSCs from these systems. The aim of this project was to develop and optimize a removal protocol for eCB-MSCs from microcarriers.

METHODS

Using 10 mL and 100 mL stirred suspension bioreactors, eCB-MSCs were expanded on microcarriers. The effects of different harvesting parameters; enzyme type and agitation rate and regime on removal efficiency and cell viability

were evaluated. The effects of enzyme type on samples obtained from 100 mL bioreactors were evaluated by exposing samples to 0.05% or 0.25% Trypsin, TrypZean, TrypLE or Accutase for 9 minutes. Harvesting efficiencies and viabilities were determined using trypan blue exclusion assay and nuclei counts respectively. In a separate study, 10 mL stirred suspension bioreactors were used to determine the effects of agitation rate and regime following enzyme treatment for full bioreactor harvests. Agitation rates of 40, 60 and 80 rpm were considered. Regimes considered included continuous agitation, semi-continuous agitation and agitating the reactor for the last minute of exposure.

RESULTS

The harvesting efficiencies for 0.05% trypsin, 0.25% trypsin, Accutase, TrypLE, and TrypZean were determined to be 11%, 44%, 35%, 35% and 27% respectively. The cell viabilities following exposure were also found to be comparable among the enzymes tested in this study.

It was also determined that the use of continuous agitation at 80 rpm resulted in the most cells being removed from a 10 mL bioreactor. These agitation rates can be scaled up for use in large bioreactors.

DISCUSSION AND CONCLUSIONS

In the large-scale production of cell therapeutics, the harvesting step is crucial to ensure high recovery of viable cells. The most effective harvesting technique was found to be 0.25% trypsin, with continuous agitation because its use resulted in significantly higher harvesting efficiency compared to other enzymes tested in this study. By testing different enzyme types and agitation rates and regimes, a better understanding of these effects on harvesting were developed. This will not only contribute to the development of a robust protocol for the harvest of eCB-MSCs, but can be applied to other cell lines grown from microcarriers for use in clinical treatments or downstream processes.

REFERENCES

1. Koch et al. *BMC Biotechnol.* **7**:26, 2007.
2. Russell et al. *PLoS One.* **10**:1-3, 2015.



EFFECTS OF LOAD CARRIAGE ON FOOT-GROUND IMPACT AND EMG ONSET TIMING IN RUNNING

Michael Esposito, Michael Baggaley, W. Brent Edwards

Human Performance Lab, Faculty of Kinesiology, University of Calgary
michael.esposito@ucalgary.ca

INTRODUCTION

Running with added mass, known as load carriage (LC) running, is an essential activity for tactical athletes. In military personnel, LC of large magnitudes (i.e., 50 lbs) is frequently required, and may be related to the high prevalence of tibial stress fractures reported in this population [1]. Retrospectively, tibial stress fractures have been linked to elevated loading rate of the vertical ground reaction force (GRF) [2]. However, no previous research has examined how vertical GRF characteristics change as a function of LC during running. Moreover, no work has investigated muscle onset timing during LC activities, which may influence GRF characteristics.

The purpose of this study was to examine how peak GRF, loading rate, muscle onset timing, and step rate are influenced by LC running. It was hypothesized that, with increased load, peak GRF, loading rate and step rate will increase, while muscle onset times will occur sooner.

METHODS

11 physically active females (19.5 ± 1.04 years, 163.77 ± 5.76 cm, 59.16 ± 7.04 kg) ran at 3.0 m/s on an instrumented treadmill (Bertec) in four loading conditions: 0, 10, 25, 50 pounds carried in a weight vest. Surface electromyography (EMG) and GRF were collected synchronously by an analog-to-digital data acquisition system at 2000 Hz (Labchart 8). EMG data were collected for the gastrocnemius, soleus, rectus femoris, vastus medialis and gluteus medius muscles.

A custom MATLAB code was used for analysis. Muscle onset time was calculated from EMG data using a double threshold method [3]. Loading rate was calculated from 20 to 80% of the line between heel strike and the impact peak of the GRF curve. Step rate was calculated as one over the time between subsequent steps. Differences in dependent variables were examined using a 1x4 repeated measure ANOVA (SPSS 24).

RESULTS

A main effect of load was observed for peak GRF, loading rate, and step rate. Post-hoc analysis revealed that peak GRF was greatest in the 50lb condition ($p < 0.001$), and no difference was observed between 10 and 25lb conditions ($p = 0.209$) (Fig. 1). Loading rate was only different between 25 and 50lb conditions ($p = 0.039$). Step rate was only different between 25 and 50lb conditions ($p = 0.01$). No change in muscle onset timing was observed as a function of load ($p \geq 0.067$).

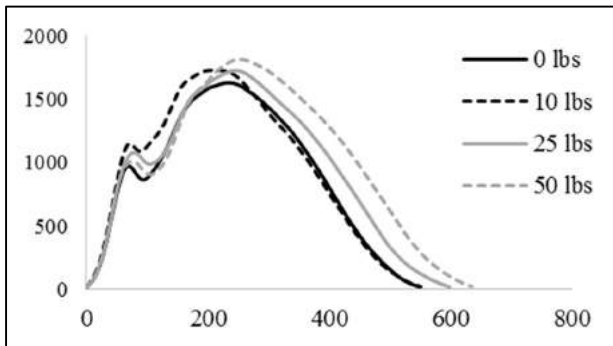


Figure.1 Ground reaction force data for all loading conditions from a representative subject. Ground reaction force in Newtons on the y-axis and stance time in milliseconds along the x-axis.

DISCUSSION AND CONCLUSIONS

The largest differences in GRF characteristics were observed in the 50lb condition. This suggests that there may be a threshold for added mass, under which individuals can maintain a relatively normal running pattern. Above this threshold, individuals likely make changes to their running pattern in an effort to reduce lower extremity loading and minimize energetic cost. However, changes observed with heavy loads suggests that internal compensation strategies may not be sufficient. External cuing to reduce step length may prove beneficial to reduce lower extremity loading in heavy load carriage conditions.

Heavy LC running may increase lower extremity injury risk due to changes in GRF characteristics.

REFERENCES

1. Milgrom et al. *Bone Joint J* **67-B**:732-5, 1985
2. Milner et al. *Med Sci Sports Exerc.* **38**:323-8, 2006.
3. Dieter et al. *Med Sci Sports Exerc.* **46**:753-761, 2014.

